





The calcium signaling module CaM-IQM destabilizes IAA-ARF interaction to regulate callus and lateral root formation

Shiqi Zhang^{a,b}, Ruixue Yu^{a,b}, Dongxue Yu^{a,b}, Pengjie Chang^{a,b}, Shiqi Guo^{a,b}, Xiaona Yang^{a,b}, Xinchun Liu^{a,b}, Chongyi Xu^{a,1} , and Yuxin Hu^{a,c,1} 

Edited by Elliot Meyerowitz, HHMI and California Institute of Technology, Pasadena, CA; received February 13, 2022; accepted May 13, 2022

Induction of a pluripotent cell mass, called callus, from detached organs is an initial step in *in vitro* plant regeneration, during which phytohormone auxin-induced ectopic activation of a root developmental program has been shown to be required for subsequent *de novo* regeneration of shoots and roots. However, whether other signals are involved in governing callus formation, and thus plant regeneration capability, remains largely unclear. Here, we report that the *Arabidopsis* calcium (Ca^{2+}) signaling module CALMODULIN IQ-MOTIF CONTAINING PROTEIN (CaM-IQM) interacts with auxin signaling to regulate callus and lateral root formation. We show that disruption of IQMs or CaMs retards auxin-induced callus and lateral root formation by dampening auxin responsiveness, and that CaM-IQM complexes physically interact with the auxin signaling repressors INDOLE-3-ACETIC ACID INDUCIBLE (IAA) proteins in a Ca^{2+} -dependent manner. We further provide evidence that the physical interaction of CaM6 with IAA19 destabilizes the repressive interaction of IAA19 with AUXIN RESPONSE FACTOR 7 (ARF7), and thus regulates auxin-induced callus formation. These findings not only define a critical role of CaM-IQM-mediated Ca^{2+} signaling in callus and lateral root formation, but also provide insight into the interplay of Ca^{2+} signaling and auxin actions during plant regeneration and development.

calcium | auxin | callus | lateral root

Plant somatic cells retain a remarkable capacity to regenerate an organ or whole individual under appropriate culture conditions (1, 2). A typical *in vitro* plant regeneration system often starts with induction of a pluripotent cell mass, termed callus, from detached organs or tissues on auxin-rich callus-inducing medium (CIM), and the auxin-induced callus formation is generally required for subsequent *de novo* regeneration of shoots and roots (1, 3, 4). Recent studies in *Arabidopsis* have revealed that auxin-induced callus formation occurs from the pericycle or pericycle-like cells within multiple organs through a root development pathway (5, 6), during which the ectopic activation of root meristematic genes is required for subsequent regeneration programs (7). Indeed, some of the INDOLE-3-ACETIC ACID-AUXIN RESPONSE FACTOR (IAA-ARF) auxin signaling modules governing lateral root formation have been shown to play a key role in directing auxin-induced callus formation. For example, *Arabidopsis* IAA3, IAA14, and IAA18 function redundantly in controlling lateral root formation by interacting with ARF7 and ARF19, and IAA19 regulates hypocotyl growth and lateral root formation by interacting with ARF7 (8–12). In agreement with this, a gain-of-function mutation in IAA14 or disruption of ARF7 and ARF19 results in a severe defect in auxin-induced callus formation (13–15). Moreover, the LATERAL ORGAN BOUNDARIES DOMAIN (LBD) transcription factors—including LBD16, LBD17, LBD29, and LBD18, which are direct or indirect targets of ARF7 and ARF19—have been shown to be key factors directing callus formation by interacting with BASIC-LEUCINE ZIPPER 59 (13, 16–18). Thus, auxin-induced ectopic activation of root developmental programs seems to represent a major type of cellular reprogramming during *in vitro* plant regeneration, and also largely determines the regeneration capability of plants. However, whether other signals are involved in governing callus-forming capacity and thus regeneration capability in plants remains largely elusive.

Calcium (Ca^{2+}) is a universal signal in all eukaryotic cells and participates in multiple cellular and developmental events. Extensive studies have established a two-step (encoding and decoding) mechanism that determines the specificity of Ca^{2+} signaling (19). The encoding mechanism entails a complex array of Ca^{2+} channels and transporters, which allow the alteration of intercellular Ca^{2+} gradients to respond to multiple environmental and developmental cues. The decoding process is characterized by a large number of Ca^{2+} sensors and effectors that convert Ca^{2+} signals into cellular effects (19). In plants, CALMODULINs (CaMs) are a family of pervasive Ca^{2+} sensors, which interact with a variety of proteins named CaM-BINDING PROTEINS (CaMBPs)—such as ion channels, kinases/

Significance

Calcium (Ca^{2+}) is a universal signal in eukaryotic cells that regulates multiple cellular and developmental events, and the link between Ca^{2+} signaling and auxin actions in plants has been considered to be missing. Here, we identified the *Arabidopsis* Ca^{2+} signaling module CALMODULIN IQ-MOTIF CONTAINING PROTEIN (CaM-IQM) as an important regulator of auxin-induced callus and lateral root formation. We further demonstrated that CaM-IQM complexes physically interact with auxin signaling repressors, INDOLE-3-ACETIC ACID INDUCIBLE (IAAs), in a Ca^{2+} -dependent manner to destabilize IAA-AUXIN RESPONSE FACTOR 7 interactions and thus modify auxin responsiveness. These findings reveal a layer of molecular interplay between Ca^{2+} signaling and auxin actions in plant regeneration and development.

Author affiliations: ^aKey Laboratory of Plant Molecular Physiology, Institute of Botany, Chinese Academy of Sciences, Beijing 100093, China; ^bUniversity of Chinese Academy of Sciences, Beijing 100049, China; and ^cNational Center for Plant Gene Research, Beijing 100093, China

Author contributions: C.X. and Y.H. designed research; S.Z., R.Y., D.Y., P.C., S.G., X.Y., and X.L. performed research; S.Z., C.X., and Y.H. analyzed data; and S.Z., C.X., and Y.H. wrote the paper.

The authors declare no competing interest.

This article is a PNAS Direct Submission.

Copyright © 2022 the Author(s). Published by PNAS. This article is distributed under Creative Commons Attribution-NonCommercial-NoDerivatives License 4.0 (CC BY-NC-ND).

¹To whom correspondence may be addressed. Email: xuchongyi@ibcas.ac.cn or huyuxin@ibcas.ac.cn.

This article contains supporting information online at <http://www.pnas.org/lookup/suppl/doi:10.1073/pnas.2202669119/-DCSupplemental>.

Published June 28, 2022.

phosphatases, metabolic enzymes, transcription factors, and chaperones—to decode specific Ca^{2+} signals (20, 21). These Ca^{2+} /CaM signaling networks have been reported to regulate plant development and responses to environmental stimuli, including root hair growth, pollen tube development, hormone response, heat-shock signaling, nitric oxide accumulation, and plant immunity (22–27). As a type of CaMBPs in plants, the IQ-MOTIF CONTAINING PROTEINs (IQMs) have been shown to be involved in regulation of plant stomatal closure, flowering, seed dormancy, and immune response (28–31). Moreover, all the basal media used for *in vitro* plant regeneration contain a certain level of Ca^{2+} (3, 32); however, whether Ca^{2+} signaling participates in plant regeneration programs remains elusive.

Here, we report that the Ca^{2+} signaling module CaM–IQM is required for auxin-induced callus and lateral root formation in *Arabidopsis*. We demonstrate that CaM–IQMs physically interact with IAA to antagonize their repressive interaction with ARF7, and thus promote auxin-induced callus formation as well as lateral root formation. Our findings define a layer of molecular interplay between Ca^{2+} and auxin signaling during plant regeneration and development.

Results

***cfc1* Is Defective in Callus and Lateral Root Formation.** We previously reported that disruption of the *Arabidopsis KCS1* gene, which encodes an enzyme, 3-ketoacyl-CoA synthase 1,

that catalyzes a rate-limiting step in the biosynthesis of very long-chain fatty acids, results in enhanced callus formation from multiple organs (15). To further identify the signals or molecules governing auxin-induced callus formation during *in vitro* regeneration of *Arabidopsis*, we performed a genetic screen with an ethylmethylsulfone (EMS)-mutagenized population of *kcs1-5*, which harbors a T-DNA insertion in *KCS1*, to identify mutants with defective or reduced callus-forming capacity when seedlings were incubated on CIM. One such mutant, initially named *callus formation capacity 1 (cfc1)*, displayed an apparent defect in callus formation from the primary roots of seedlings on CIM when compared with *kcs1-5* or WT (Fig. 1A). To examine the effect of the *cfc1* mutation on the callus-forming capacity of other organs, we incubated hypocotyl and cotyledon explants of WT, *kcs1-5*, and *cfc1* on CIM, and observed that callus formation in the *cfc1* explants was also dampened (Fig. 1A), indicating that *cfc1* impedes callus-forming capacity of multiple organs.

As auxin-induced callus formation occurs from pericycle or pericycle-like cells through a root development pathway (6), we crossed the pericycle marker line J0121 of Col-0 background (15, 33) with the *kcs1-5* and *cfc1* mutants and obtained the respective F3 progenies homozygous in both J0121 marker and mutant background, and next compared the fluorescent signals in the pericycle cells and resulting calli in the primary roots of WT, *kcs1-5*, and *cfc1* seedlings. Before seedlings were incubated on CIM, comparable J0121 signals were observed in the

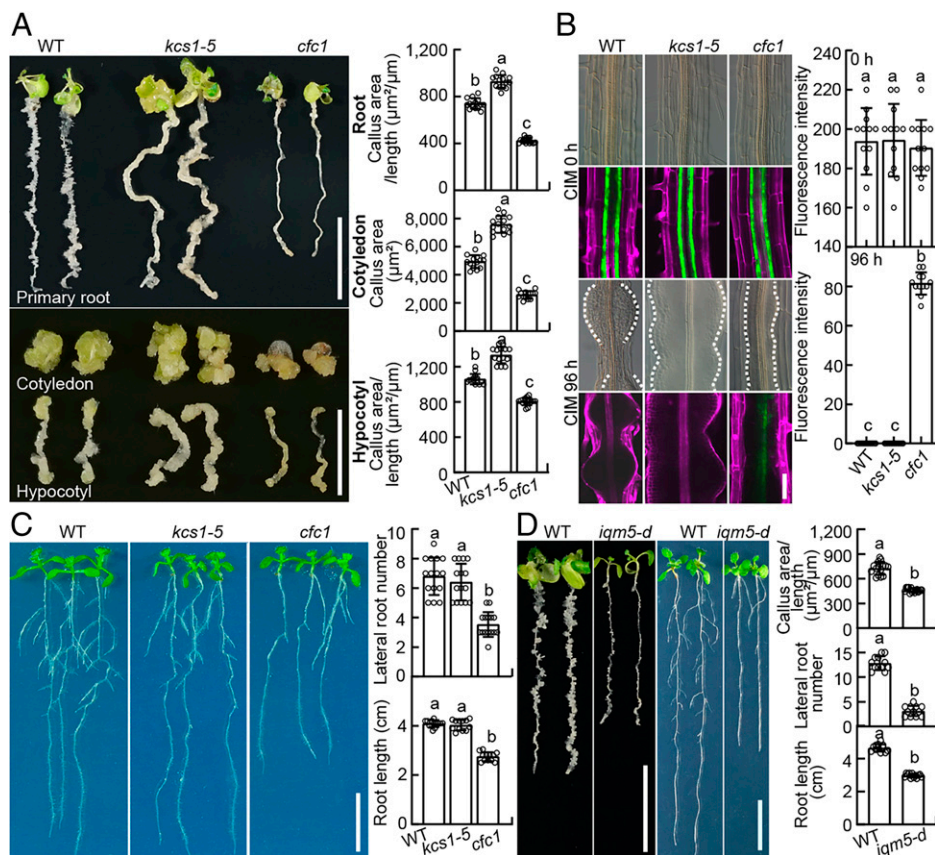


Fig. 1. A mutation in IQM5 impedes callus and lateral root formation. (A) Callus-forming phenotype in the primary roots and cotyledon and hypocotyl explants of WT, *kcs1-5*, and *cfc1* seedlings. The 7-d-old seedlings or cotyledon and hypocotyl explants were incubated on CIM for 12 or 20 d and the areas of formed callus were determined ($n = 14$). (Scale bars, 10 mm.) (B) Cytochemistry of pericycle and resulting calli in the mature zone of WT, *kcs1-5*, and *cfc1* primary roots. The morphology of the pericycle or calli and expression of pericycle marker J0121 were visualized in 7-d-old seedlings on CIM for 0 or 96 h (Left), and the GFP fluorescent signals of J0121 were quantified ($n = 12$) (Right). (Scale bar, 50 μm .) (C) Morphology of 10-d-old WT, *kcs1-5*, and *cfc1* seedlings. The lateral root number ($n = 15$) and primary root length ($n = 12$) are shown. (Scale bar, 10 mm.) (D) Callus- and lateral root-forming phenotypes of WT and *iqm5-d* seedlings. Callus area ($n = 15$), lateral root number ($n = 12$), and primary root length ($n = 12$) are shown. (Scale bar, 10 mm). Data are presented as means \pm SD. Different letters indicate significant differences at $P < 0.05$ determined by one-way ANOVA with Tukey's multiple comparison test.

pericycle cells of WT, *kcs1-5*, and *cfc1* roots (Fig. 1B). After seedlings were incubated on CIM for 96 h, active callus formation occurred from the pericycle cells of WT and *kcs1-5* roots where the J0121 signals almost disappeared; however, callus formation from the *cfc1* pericycle was apparently delayed, as the J0121 signal was still detectable (Fig. 1B). Notably, unlike the lateral root primordium-like calli formed from WT pericycle, continuous callus formation was observed from a whole layer of the *cfc1* pericycle and from the *kcs1-5* pericycle (Fig. 1B), implicating that the effect of *cfc1* on callus formation is independent of the *kcs1-5* mutation. Moreover, the *cfc1* seedlings were also defective in lateral root initiation and developed shorter primary roots than *kcs1-5* and WT (Fig. 1C), and growth and development of *cfc1* plants were also retarded (SI Appendix, Fig. S1A). These observations demonstrate that the mutation in *cfc1* impairs callus and lateral root formation as well as plant development.

IQMs Function Redundantly in Regulating Callus Formation.

To identify the gene responsible for the *cfc1* phenotype, we backcrossed *cfc1* with *kcs1-5* and examined the callus-forming phenotype in the F₂ generation on CIM. We found that the F₂ seedlings segregated for the *kcs1-5*, intermediate, and *cfc1* phenotypes in a ratio of 1:2:1 (53:119:49; $\chi^2 = 0.1189$) (SI Appendix, Fig. S1B), demonstrating that the *cfc1* phenotype is caused by a semidominant mutation of a single gene. Using a map-based cloning approach with an F₂ population obtained from the cross of *cfc1* with the Landsberg *erecta* (Ler) accession (34), we mapped the *cfc1* mutation to a 160-kb region on chromosome 5, in which a transition of G-to-A was identified in the coding region of *At5g57010*, which led to a premature truncation of the IQM5 with 426 amino acids (SI Appendix, Fig. S1C). To further verify that this mutation is responsible for the *cfc1* phenotype, we introduced the IQM5 coding sequence driven by the CaMV35S promoter or its native promoter into *cfc1*, respectively. As expected, constitutive overexpression of IQM5 driven by the CaMV35S promoter fully rescued the callus-forming defect of the *cfc1* seedlings (SI Appendix, Fig. S1D), whereas introduction of IQM5 driven by its native promoter led to a partial or full rescue of callus formation among different *cfc1* individuals (SI Appendix, Fig. S1E). These findings confirm that the IQM5 mutation in the *cfc1* mutant has a dominant effect and is responsible for the callus-formation defect. Next, we crossed *cfc1* with WT and obtained a mutant without *kcs1-5*, designated as *iqm5-d*. As expected, the *iqm5-d* seedlings still displayed a reduced callus-forming capacity in their primary roots on CIM and developed short primary roots with fewer lateral roots when compared with WT (Fig. 1D), further supporting the notion that the effect of *iqm5-d* on callus formation is independent of *kcs1-5*.

Next, we obtained a loss-of-function mutant of IQM5, *iqm5-1* (SALK_134786), in which a T-DNA was inserted in the first exon and disrupted the transcription of IQM5 (31) (SI Appendix, Fig. S1C). Interestingly, the *iqm5-1* seedlings incubated on CIM did not have an obvious callus-forming defect when compared with WT (SI Appendix, Fig. S2A). As the *Arabidopsis* IQM family contains six members—among which the IQM5, IQM1, and IQM4 belong to a phylogenetic clade (35) (SI Appendix, Fig. S2B)—we thus speculated that some IQM members might function redundantly with IQM5 in regulating callus formation. Transcriptional analysis revealed that both IQM5 and IQM1 were highly responsive to CIM (SI Appendix, Fig. S2C), and IQM5 and IQM1 were found to abundantly accumulate in the pericycle cells of primary roots and the

resulting calli (SI Appendix, Fig. S2D). We thus obtained the T-DNA insertion mutant *iqm1-1* (SALK_127727), in which the transcription of IQM1 was disrupted (29, 36) (SI Appendix, Fig. S2E). As expected, like *iqm5-1*, the *iqm1-1* seedlings on CIM did not show any obvious callus-forming defect, while apparently dampened callus formation was observed in the primary roots of the *iqm1-1 iqm5-1* double mutant, and this callus-forming defect could be rescued by introduction of a native promoter-driven IQM1 (SI Appendix, Fig. S2A). Therefore, we conclude that IQM5 and IQM1, possibly together with other IQM members, function redundantly in governing callus formation.

CaM-IQM-Mediated Calcium Signaling Is Required for Callus Formation.

As IQMs belong to a family of CaMBPs and can interact with CaMs in a Ca²⁺-independent manner to decode Ca²⁺ signals (29), we reasoned that the Ca²⁺ signaling module CaM-IQMs are involved in regulation of callus formation. To test this, we first determined which of the seven *Arabidopsis* CaM members (37) could physically interact with IQM5 or IQM1. Yeast two-hybrid assays showed that IQM5 could interact with CaM3, CaM5, and CaM6, while IQM1 interacted with CaM5 and CaM6 (SI Appendix, Fig. S3A). Further luciferase complementation imaging (LCI) assays performed in *Nicotiana benthamiana* leaves revealed that both IQM5 and IQM1 interacted with CaM3, CaM5, and CaM6 *in planta* (SI Appendix, Fig. S3B). Moreover, using transgenic plants harboring a *pCaM3::CaM3-GFP*, *pCaM5::CaM5-GFP*, or *pCaM6::CaM6-GFP* construct, we showed that CaM3, CaM5, and CaM6 accumulated abundantly in the pericycle or resulting callus (SI Appendix, Fig. S3C), indicating that these CaM members are potential partners of IQM5 and IQM1 during callus formation.

Next, we obtained a T-DNA insertion mutant of *CaM5*, *cam5-4* (SALK_027181) (37), with disrupted *CaM5* transcription (SI Appendix, Fig. S3D). As mutants for *CaM6* and *CaM3* were publicly unavailable, we generated two allelic mutants in each gene by CRISPR/Cas9 approach, and designated as the *cam6-1*, *cam6-2* and *cam3-1*, *cam3-2*, respectively (SI Appendix, Fig. S3E). Interestingly, *cam6-1* and *cam6-2* seedlings but not the *cam5-4*, *cam3-1*, and *cam3-2* seedlings on CIM exhibited a callus-forming phenotype distinguishable from that of WT, and this callus-forming defect in *cam6-1* could be restored by introduction of a *pCaM6::CaM6-GFP* construct (SI Appendix, Fig. S3F and G). Next, we generated the double-mutants *cam3-1 cam5-4*, *cam3-1 cam6-1*, and *cam5-4 cam6-1*, and the triple-mutant *cam3-1 cam5-4 cam6-1*, and observed that the callus-forming defect of *cam6-1* seedlings could be enhanced by *cam5-4* but not by *cam3-1* (SI Appendix, Fig. S3F), demonstrating that CaM6 and CaM5 govern callus formation in a partially redundant manner.

To further define the involvement of CaM-IQM-mediated Ca²⁺ signaling in callus and lateral root formation, we compared the callus-forming phenotypes of WT, *cam6-1*, *iqm5-d*, and *cam6-1 iqm5-d* seedlings on CIM with or without Ca²⁺. As expected, an increase of Ca²⁺ concentration in CIM promoted callus formation from WT roots in a dose-dependent manner, whereas the effect of Ca²⁺ was obviously attenuated in the *cam6-1*, *iqm5-d*, and *cam6-1 iqm5-d* roots (Fig. 2A). Similarly, Ca²⁺ also promoted lateral root formation in WT seedlings in a dose-dependent manner, and this response was largely dampened in the *cam6-1*, *iqm5-d*, and *cam6-1 iqm5-d* seedlings (SI Appendix, Fig. S3H). In addition, the callus- and lateral root-forming phenotypes of *cam6-1 iqm5-d* resembled those of

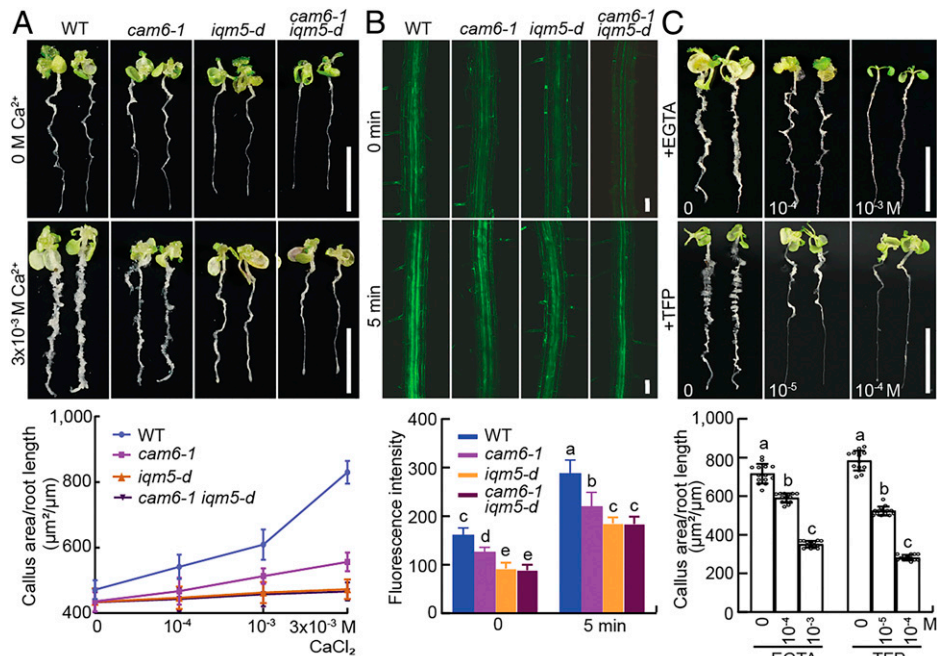


Fig. 2. CaM-IQM modules are required for auxin-induced callus formation. (A) Callus-forming phenotypes of WT, *cam6-1*, *iqm5-d*, and *cam6-1 iqm5-d* seedlings on CIM supplemented with the indicated concentrations of CaCl_2 for 12 d ($n = 12$). (Scale bars, 10 mm.) (B) *GCaMP6s::GFP* fluorescent signals visualized in the primary roots of WT, *cam6-1*, *iqm5-d*, and *cam6-1 iqm5-d* seedlings. The 7-d-old seedlings were incubated in liquid CIM for 0 and 5 min, and the GFP fluorescence was quantified ($n = 12$). (Scale bars, 50 μm .) (C) Effect of the Ca^{2+} chelator EGTA and CaM antagonist TFP on callus-forming capacity. The 7-d-old WT seedlings were incubated on CIM supplemented with the indicated concentrations of EGTA ($n = 14$) or TFP ($n = 15$) for 12 d. (Scale bars, 10 mm.) Data are shown as means \pm SD. Different letters indicate significant differences at $P < 0.05$ determined by one-way or two-way ANOVA with Tukey's multiple comparison test.

iqm5-d (Fig. 2A and *SI Appendix*, Fig. S3H), supporting that CaM and IQM function in a same-signaling module. Furthermore, we observed that the signals of *GCaMP6s::GFP*, an in vivo indicator of intracellular Ca^{2+} response (38), were comparatively weaker in the *cam6-1*, *iqm5-d*, and *cam6-1 iqm5-d* roots than in the WT roots before and after the seedlings were incubated with CIM (Fig. 2B). In contrast, supplementation of CIM with the calmodulin antagonist trifluoperazine (TFP) or Ca^{2+} chelator ethylene glycol tetraacetic acid (EGTA) obviously inhibited callus formation from WT roots, which recapitulated the callus-forming defect observed in *iqm5-d* (Fig. 2C). Taking these data together, we conclude that CaM-IQM-mediated calcium signaling plays a critical role in regulating callus and lateral root formation.

Disruption of CaM-IQM Dampens Auxin Responsiveness.

Given that auxin plays a key role in directing callus and lateral root formation (3, 4, 13), we investigated whether CaM-IQM modules could impact auxin responsiveness. We first compared lateral root formation among WT, *cam6-1*, *iqm5-d*, and *cam6-1 iqm5-d* seedlings in response to exogenous auxin. As expected, when seedlings were treated with the low concentrations of 1-naphthylacetic acid (NAA), lateral root formation was induced in WT seedlings in a dose-dependent manner; however, the induction of lateral root formation by NAA was obviously dampened in the *cam6-1*, *iqm5-d*, and *cam6-1 iqm5-d* seedlings (*SI Appendix*, Fig. S4A). Consistent with this, fluorescent signals of the *DR5::GFP*, a well-used indicator of auxin response (39), were weaker in the *cam6-1*, *iqm5-d*, and *cam6-1 iqm5-d* roots than in WT roots, either with or without treatment with the natural form of auxin IAA (*SI Appendix*, Fig. S4B). These observations illustrate that disruption of the CaM-IQM module attenuates auxin responsiveness.

To further verify the impact of CaM-IQM modules on auxin responsiveness, we also monitored the transcription of

early auxin-responsive genes—namely *IAA5*, *IAA14*, *IAA19*, *IAA28*, and *IAA29* (40), as well as *LBD16*, *LBD17*, and *LBD29*—that act downstream of the auxin signaling module IAA-ARF to direct callus and lateral root formation (13), in the WT, *cam6-1*, *iqm5-d*, and *cam6-1 iqm5-d* seedlings after treatment with IAA. As expected, compared with that in WT, the transcriptional induction of *IAA5*, *IAA14*, *IAA19*, *IAA28*, and *IAA29* by exogenous IAA was obviously attenuated in the *cam6-1*, *iqm5-d*, and *cam6-1 iqm5-d* seedlings (*SI Appendix*, Fig. S4C). Likewise, the IAA-induced transcription of *LBD16*, *LBD17*, and *LBD29* was also reduced in these mutant genotypes (*SI Appendix*, Fig. S4C). These results support that CaM-IQM modules are required for proper auxin responsiveness during callus and lateral root formation.

CaMs Physically Interact with IAAs in a Ca^{2+} -Dependent Manner.

Because CIM contains a high level of the synthetic auxin analog 2,4-dichlorophenoxyacetic acid (2,4-D), and 2,4-D has been shown to not require auxin efflux carriers for polar transport (4, 41), we thus reasoned that the auxin responsiveness mediated by CaM-IQM during callus induction is likely attributable to the alteration of auxin signaling rather than polar transport or homeostasis. Since auxin signaling is mainly mediated by the $\text{SCF}^{\text{TIR1/AFB}}$ complex via targeting the downstream signaling repressor IAA proteins for proteolytic degradation (42, 43), we thus performed a yeast two-hybrid assay with IQM5 and CaM6 to test whether IQM and CaM physically interact with key auxin signaling components, including TRANSPORT INHIBITOR RESPONSE 1 (TIR1), AUXIN SIGNALING F-BOX 2 (AFB2), AFB3, S PHASE KINASE-ASSOCIATED PROTEIN 1 (SKP1), and IAA members involved in callus and lateral root formation, such as *IAA5*, *IAA14*, *IAA19*, *IAA28*, and *IAA29*. We failed to detect any physical interaction between IQM5 and these auxin signaling factors (*SI Appendix*, Fig. S5A), but physical interactions

between CaM6 and AFB2, AFB3, and IAA19 were detectable in yeast cells (*SI Appendix, Fig. S5B*). Furthermore, physical interactions between CaM5 and AFB2, AFB3, and IAA19 were also detected in yeast cells (*SI Appendix, Fig. S5C*). To verify the interactions of CaM5 and CaM6 with AFB2, AFB3, and IAA members *in planta*, we conducted an LCI assay in *N. benthamiana* leaves, and found that both CaM6 and CaM5 only interacted with IAA19 and IAA28 (Fig. 3A). The interaction of CaM6 with IAA19 was further validated by a coimmunoprecipitation (co-IP) assay (Fig. 3B).

As the physical interaction of CaM and IQM has been shown to be independent of Ca²⁺ (29), we thus investigated whether the interaction of CaM6 and IAA19 is Ca²⁺-dependent and whether IQMs are required for this interaction. Indeed, co-IP assays performed with transgenic plants coexpressing epitope-tagged IAA19 and CaM6 clearly showed that Ca²⁺ treatment could induce the physical interaction of CaM6 and IAA19 and that the effect of Ca²⁺ was dose-dependent (Fig. 3C). In contrast, the physical interaction of CaM6 and IAA19 could be largely disrupted by EGTA treatment and in the *iqm5-d* background (Fig. 3D), demonstrating that both Ca²⁺ and IQMs are required for the physical interaction of CaM6 and IAA19.

CaM6 Destabilizes the Interaction between IAA19 and ARF7.

Since most IAAs function as auxin signaling repressors by interacting with ARFs to repress their transcriptional activities, and

IAA19 has been reported to physically interact with ARF7 to inhibit lateral formation (10), we speculated that the interaction of CaMs and IAA19 might modify auxin signaling either by affecting IAA19 stability or by antagonizing its interaction with ARF7. To test this, we first compared IAA19 accumulation among WT, *cam6-1*, *iqm5-d*, and *cam6-1 iqm5-d* seedlings harboring a *pIAA19::IAA19-GFP* construct, but found that the subcellular localization of IAA19 and its abundance in the primary roots were comparable among these four genotypes (*SI Appendix, Fig. S6A*). We also generated transgenic plants harboring a *pIAA19::mIAA19-GFP* construct, which expressed a gain-of-function mutated isoform of IAA19 (mIAA19) that cannot be degraded by auxin-induced proteolysis in the *mas-sugu2-1* (*msg2-1*) background (10, 44), and monitored the accumulation of IAA19 and mIAA19 in response to Ca²⁺. Indeed, the abundance of mIAA19 was found to be much higher than that of IAA19 in the transgenic seedlings, while Ca²⁺ treatment did not affect the abundance of either IAA19 or mIAA19 (*SI Appendix, Fig. S6B*). These observations exclude the possibility that physical interaction of CaM6 and IAA19 affects IAA19 abundance or stability. Consistent with this, *msg2-1* seedlings on CIM still exhibited some degree of callus formation in response to Ca²⁺ (*SI Appendix, Fig. S6C*).

Next, we tested whether CaM6 could antagonize ARF7 to interact with IAA19. Both LCI and co-IP assays clearly showed that ARF7 physically interacted with IAA19 and mIAA19, and

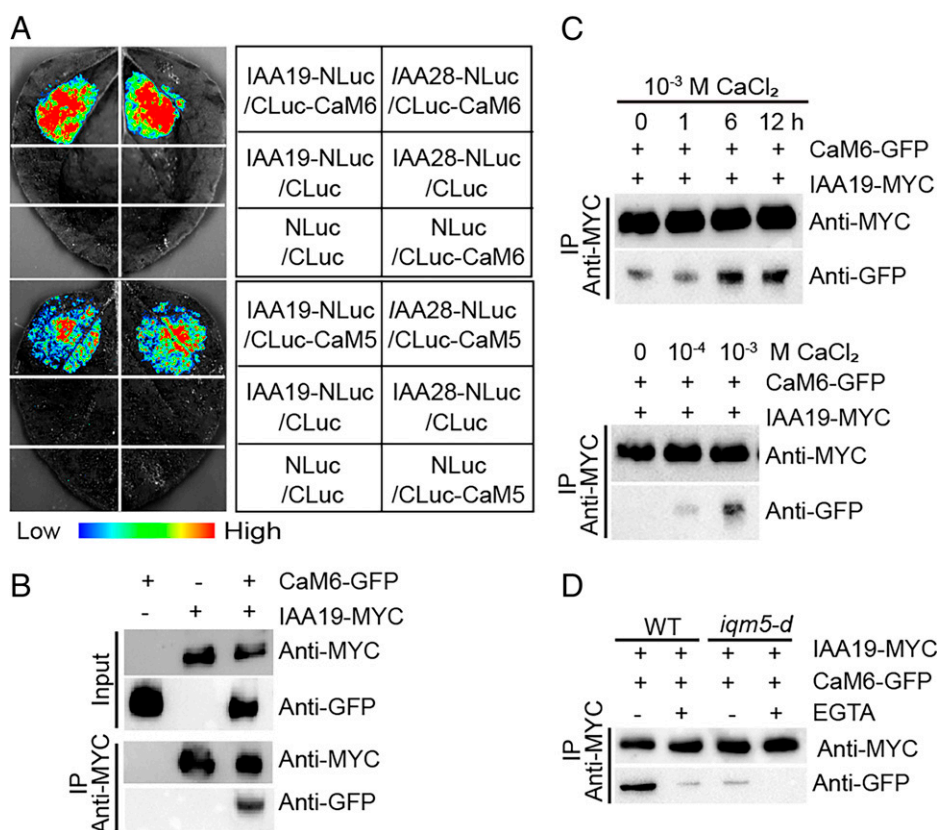


Fig. 3. Physical interactions of CaMs and IAAs are Ca²⁺- and IQM-dependent. (A) Physical interaction of CaM6 or CaM5 with IAA19 or IAA28 was assayed by LCI in *N. benthamiana* leaves. Representative images of leaves coexpressing CLuc-CaM5 or CLuc-CaM6 and/or IAA19-NLuc or IAA28-NLuc are shown. (B) Co-IP assays of the interaction of CaM6 and IAA19. IAA19-MYC and/or CaM6-GFP proteins transiently expressed in *N. benthamiana* leaves were immunoprecipitated by an agarose-conjugated anti-MYC matrix and immunoblotted with anti-GFP and anti-MYC antibodies. The experiments were performed in two biological replicates. (C) Ca²⁺ induces the physical interaction of CaM6 and IAA19. Co-IP assay was performed with transgenic WT seedlings expressing IAA19-MYC and CaM6-GFP incubated in B5 medium supplemented with 10⁻³ M CaCl₂ for the indicated times (*Upper*) or with indicated CaCl₂ concentrations for 1 h (*Lower*). The experiments were performed in two biological replicates. (D) Ca²⁺ and IQMs are required for interaction of CaM6 and IAA19. Co-IP assay was performed with transgenic WT and *iqm5-d* seedlings expressing IAA19-MYC and CaM6-GFP treated with or without 1 mM EGTA for 1 h. The experiments were performed in three biological replicates.

that the interaction of ARF7 with IAA19 or mIAA19 was remarkably antagonized by the coexpression of CaM6 (Fig. 4 A and B). This might explain why callus formation is still inducible by Ca²⁺ in *msg2-1* seedlings (SI Appendix, Fig. S6C). Consistent with this, a yeast two-hybrid assay revealed that CaM6 could physically interact with the C terminus of IAA19 (SI Appendix, Fig. S6D), which is required for physical interaction with ARFs (10, 45, 46). Thus, the derepression of ARF7 by CaMs seems to be a possible mechanism behind the interplay of CaM-IQM and auxin signaling. To test this, we first examined whether Ca²⁺ could elevate the transcription of *LBD16* and *LBD29*, two genes directly targeted by ARF7 (17). As expected, the transcript abundances of *LBD16* and *LBD19* were obviously increased by Ca²⁺ treatment (Fig. 4C). Next, we overexpressed *ARF7* in the *iqm5-d* mutant, and observed that overexpression of *ARF7* could partially restore callus formation in the *iqm5-d* seedlings (Fig. 4D), supporting that ARF7 is genetically downstream of the CaM-IQM module in directing callus formation. We thus conclude that the physical interaction of CaM6 with IAA19 releases ARF7 activity and thus promotes callus formation.

Discussion

Recent studies in *Arabidopsis* have revealed that two types of cellular reprogramming occur during plant organ repair and regeneration: auxin-induced callus formation and wound-induced cell dedifferentiation (6, 13, 47, 48). Because CIM contains a high level of auxin, and auxin-induced ectopic activation of root meristematic genes is required for subsequent de novo shoot or root regeneration (5–7, 49), it is likely that auxin-induced callus formation represents a major cellular event in the acquisition of regeneration capability during in vitro plant regeneration. Accumulating evidence indicates

that auxin-induced callus formation shares a developmental program with lateral root formation, and that some of the key auxin signaling components involved in lateral root formation are required for callus formation (6, 7, 13). However, it is yet unclear whether Ca²⁺ signaling plays a role in the callus-forming program. Here, we demonstrate that Ca²⁺ signaling module CaM-IQM plays an important role in auxin-induced callus and lateral root formation by modifying auxin signaling module IAA-ARFs, which defines a layer of molecular interplay between Ca²⁺ and auxin signaling during in vitro plant regeneration and development. Obviously, as both Ca²⁺ and auxin are endogenous signals of plants, the modification of IAA-ARFs by CaM-IQM module wouldn't be an immediate "all-or-none" but a step-wise process with concurrent activation of ARFs in response to Ca²⁺. It is likely that, under normal growth conditions, a low Ca²⁺ gradient in the pericycle is perceived by a CaM-IQM complex for interacting with IAA proteins to relieve the ARF activity, and such low Ca²⁺ signature coordinates with endogenous auxin signaling to allow proper lateral root initiation. Upon CIM treatment, high levels of auxin and Ca²⁺ lead to a high Ca²⁺ gradient in the pericycle or pericycle-like cells, and this high Ca²⁺ signature is perceived by CaM-IQMs to derepress IAA-inhibited ARF activities, which synergizes with auxin-induced IAA proteolysis to ectopically activate the root developmental program and thus callus formation (SI Appendix, Fig. S7).

Ca²⁺ signaling participates in multiple cellular responses to external cues (50–52). Previous studies have revealed that auxin is a potential inducer of Ca²⁺ waves and that intracellular Ca²⁺ fluctuation also results in a homeostatic change of endogenous auxin through modification of auxin biosynthesis and transport. For example, an increase of cytosolic Ca²⁺ by phytosulfokine perception activates auxin biosynthesis via interaction between CaMs and YUCCA (53), while mechanic-stimulated transient

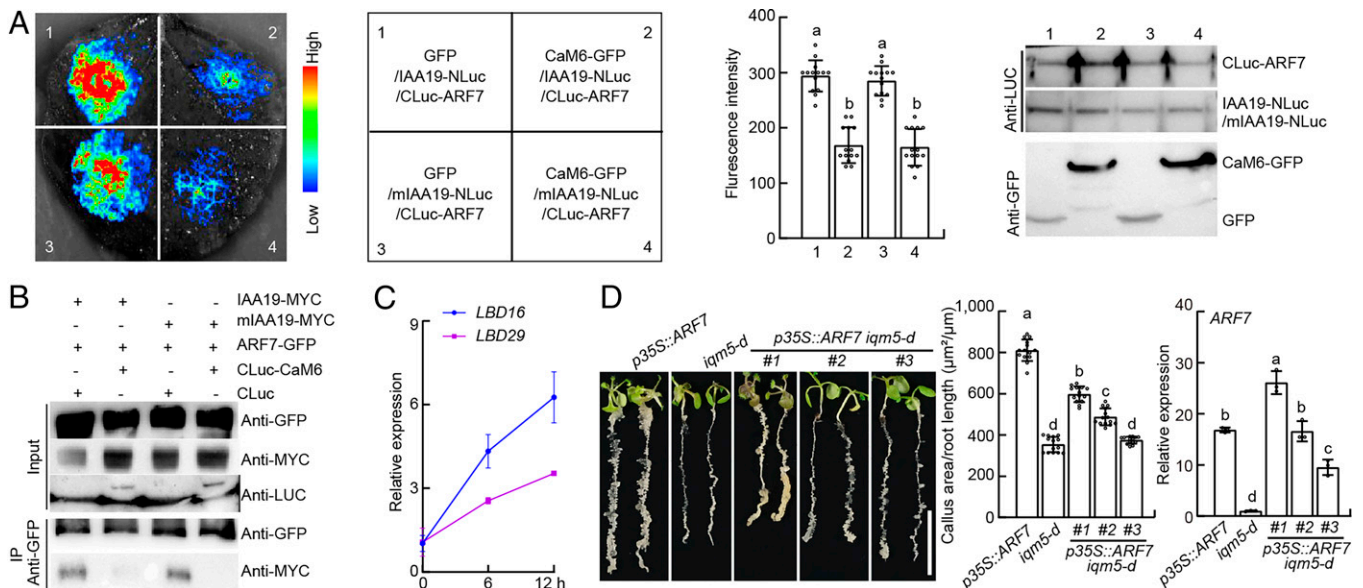


Fig. 4. CaM6 destabilizes the ARF7-IAA19 interaction. (A) CaM6 dampens ARF7-IAA19 interaction. LCI assay was performed with *N. benthamiana* leaves transiently coexpressing Cluc-ARF7 and IAA19/mIAA19-NLuc with GFP (empty vector) or CaM6-GFP. Representative images of an infiltrated leaf, the coexpressed proteins, the quantified fluorescent signals ($n = 15$), and the immunoblotted protein abundances are shown from left to right. (B) CaM6 destabilizes the physical interaction of ARF7 and IAA19. Co-IP assay was performed with *N. benthamiana* leaves transiently expressing ARF7-GFP and IAA19-MYC or mIAA19-MYC with Cluc-CaM6 or CLuc (empty vector) using an agarose-conjugated anti-GFP matrix and immunoblotting with anti-GFP and anti-MYC antibodies. The experiments in A and B were performed for at least two biological replicates. (C) Transcriptional induction of *LBD16* and *LBD29* by Ca²⁺. qRT-PCR was performed with 7-d-old WT seedlings incubated on B5 medium containing 10⁻³ M CaCl₂ for 0, 6, and 12 h ($n = 3$ biological replicates). (D) Overexpression of *ARF7* partially rescued the callus-forming defect of the *iqm5-d* roots. The 7-d-old seedlings of *p35S::ARF7*, *iqm5-d*, and three independent *p35S::ARF7 iqm5-d* lines were incubated on CIM for 12 d, and the area of callus formed in primary roots ($n = 14$) and the transcript abundances of *ARF7* ($n = 3$ biological replicates) were determined. (Scale bar, 10 mm.) Data are presented as means \pm SD. Different letters indicate significant differences at $P < 0.05$ determined by one-way ANOVA with Tukey's multiple comparison test.

changes in Ca^{2+} in the plant stem cell niche alters the polarity of PIN-FORMED1 (54). The *Arabidopsis* CALCINEURIN B-LIKE PROTEIN-INTERACTING PROTEIN KINASE 6 participate in lateral root formation, as well as callus formation, by affecting auxin transport (55, 56). Although a few lines of evidence have suggested that Ca^{2+} or CaM signaling affects auxin response (27, 57, 58), little is yet known about the interplay of Ca^{2+} and auxin at the signaling level. Therefore, the link of Ca^{2+} signaling and auxin actions has been considered to be still missing (59). Here, we provide substantial evidence that the Ca^{2+} signaling module CaM–IQM interacts with the key auxin signaling component IAA–ARF by antagonistically interacting with IAAAs, and thus regulating callus and lateral root formation. Interestingly, although IQM forms a complex with CaM via its N-terminal IQ-motif (29), our finding that the truncated IQM5 protein in *iqm5-d* had a dominant effect strongly suggests that the C-terminal regions of IQMs are essential for the CaM–IQM module to decode Ca^{2+} signals. Moreover, as both IAAAs and ARFs act largely redundantly in auxin signaling (43), and we only identified IAA19–ARF7 as a physical target of the CaM–IQM module, it is possible that other IAAAs, including IAA28, or ARFs are also the potential targets of CaM–IQM modules during auxin-regulated regeneration and development. On the other hand, since CaMs decode specific Ca^{2+} signals by forming multiple complexes with various types of CaMBPs, it is also plausible that similar CaM–IAA interactions might exist in these Ca^{2+} signaling modules to modify auxin actions during plant development and environmental responses. Therefore, further work on these interactions will shed light on the molecular links between Ca^{2+} signaling and auxin actions.

Finally, although auxin-induced callus formation is an initial step in *in vitro* plant regeneration and largely determines the regeneration capacity of the plant, we still know little about how the varied regeneration capacities are determined among different plant species. In *Arabidopsis*, *ABERRANT LATERAL ROOT FORMATION* (*ALF4*), which encodes a nuclear protein initially identified to be required for lateral root formation, has been shown to be essential for callus formation (6, 60), as disruption of *ALF4* leads to the loss of callus-forming capability in multiple organs, including roots, cotyledons, and petals (6). A recent study showed that, although *ALF4* is not responsive to auxin, the *ALF4* protein could bind to RING BOX 1 (RBX1), a subunit of the SCF^{TIR1} complex, to inhibit the activity of SCF^{TIR1} and thus affect auxin sensitivity (61). Recently, very long-chain fatty acids or their derivatives have been defined as restrictive signals limiting callus-forming capability, at least in part, by modulating transcription of *ALF4* (15). Interestingly, we demonstrate here that the Ca^{2+} signaling module CaM–IQM regulates callus-forming capacity by modifying the interaction of IAA–ARFs and thus auxin response. It seems that auxin response or sensitivity might be one of the molecular mechanisms behind callus-forming capacity. Thus, further identification of signals or factors governing callus formation will be necessary to clarify how regeneration capability is determined in plants.

Materials and Methods

Plant Materials and Growth Conditions. The *Arabidopsis thaliana* Columbia-0 accession was used in this study. The T-DNA insertion mutants *iqm5-1* (SALK_134786), *iqm1-1* (SALK_127727), and *cam5-4* (SALK_027181) were obtained from the *Arabidopsis* Biological Resource Center (ABRC) and verified by PCR analyses, as described previously (30, 31, 37). The *Arabidopsis* J0121, *DR5::GFP*, and *GCaMP6s::GFP* marker lines and *msg2-1* mutant were

described previously (10, 33, 38, 39). The *Arabidopsis* seeds were surface-sterilized in ~1% sodium hypochlorite, rinsed three times with sterile water, and germinated on half-strength Murashige and Skoog medium (3) (1/2 MS medium; Coolaber), 1% sucrose, 0.5% plant agar (pH 5.7) after stratification at 4 °C for 2 d. The seedlings and plants were grown in a culture room or growth chamber at 22 ± 2 °C with a 16/8-h light/dark photoperiod and an illumination intensity of 80 to 90 $\mu\text{mol m}^{-2}\text{s}^{-1}$.

EMS Mutagenesis and CRISPR/Cas9 Editing. EMS mutagenesis was carried out according to the method described previously (62). The *kcs1-5* seeds were immersed in 100 mM phosphate buffer (pH 7.5) for 3 d at 4 °C and dried on filter paper for 1 d. The seeds were subsequently mutagenized in 100 mM phosphate buffer containing 0.4% (vol/vol) EMS (Sigma) at room temperature for 8 h, and then washed three times with sterilized water. The mutagenized seeds (M1 generation) were grown in soil and allowed to self-pollinate. The seeds of M1 plants (M2 generation) were collected and germinated in 1/2 MS medium. The 7-d-old seedlings were transferred on CIM, and callus formation in the primary roots was examined at 7 d. The candidate *clc* mutants were transferred onto 1/2 MS medium for recovery and then grown in soil, and their callus-forming phenotypes were further validated in the M3 generation.

To generate the *cam3* and *cam6* allelic mutants, an *Arabidopsis* egg cell-specific promoter-controlled CRISPR/Cas9 gene-editing system was used as previously described (63). Briefly, the 23-bp specific target sequences with PAM sites (5'-N20NGG-3') were manually identified within the exons of *CAM3* and *CaM6*, and their specificities were evaluated using the BLAST tool on the TAIR website (<https://www.arabidopsis.org/Blast/index.jsp>). Primers corresponding to these gRNAs were designed (SI Appendix, Table S1), and PCR was performed using the pCBC-DT1T2 plasmid as a template. The PCR products were cloned into the pHEE401 vector and transformed into *Arabidopsis*. Mutations within the target genes were identified in the transgenic T1 plants, and the homozygous T3 plants without the construct were identified by sequencing and used for further characterization.

Callus Induction and Lateral Root Formation. For characterization of the callus-forming phenotype, 7-d-old seedlings or their explants were incubated on CIM (B5 medium [Coolaber], 2% glucose, 0.5% MES, 0.25% phytagel supplemented with 2.26 μM 2,4-D, and 0.23 μM kinetin, pH 5.7) (7) for 12 or 20 d. To examine the effect of Ca^{2+} on callus formation, the 7-d-old seedlings were cultured on CIM without or with different concentrations of CaCl_2 (Sigma) or on CIM supplemented various concentrations of EGTA (Sigma) or TFP (Sigma) for 12 d. The formed callus was photographed and the area of callus was quantified with ImageJ software (15). To characterize lateral root formation, the seedlings were grown on 1/2 MS medium for 10 d, or the 5-d-old seedlings were transferred to 1/2 MS supplemented with various concentrations of NAA for 12 h or to 1/2 MS with or without CaCl_2 for 5 d, and the numbers of lateral root initiates were counted under a stereoscope. All experiments above were repeated for at least 3 independent biological replicates with more than 12 independent plants each time.

Plasmid Construction and Arabidopsis Transformation. For generation of the transgenic plants, a genomic *IQM5* fragment containing a 1,464-bp promoter and a 1,997-bp coding region, an *IQM1* fragment containing a 2,103-bp promoter and a 2,130-bp coding region, and a genomic *CaM6* fragment containing a 1,518-bp promoter and a 1,208-bp coding region were fused with a *GFP* sequence and cloned into the pCambia1300 plasmid (Cambia) to generate the *pIQM5::IQM5-GFP*, *pIQM1::IQM1-GFP*, and *pCaM6::CaM6-GFP* constructs, respectively. The cDNA fragments of *IQM5* and *ARF7* were cloned into the pSuper1300 vector to generate the *p35S::IQM5* and *p35S::ARF7* constructs, respectively. For determination of the tissue-specific expression of CaMs and IAA19, a DNA fragment of *CaM3* containing a 1,072-bp promoter and a 940-bp coding sequence, *CaM5* containing a 1,851-bp promoter and a 2,108-bp coding sequence, and the DNA fragments of *IAA19* from WT or *msg2-1* containing a 2,038-bp promoter and a 594-bp coding sequence were fused with a *GFP* sequence and cloned into the pCambia1300 plasmid for generation of *pCaM3::CaM3-GFP*, *pCaM5::CaM5-GFP*, *pIAA19::IAA19-GFP*, and *pIAA19::miIAA19-GFP*, respectively. All the plasmids were verified by sequencing and introduced into the *Agrobacterium tumefaciens* strain EHA105 or ABI and transformed into *Arabidopsis* by the standard floral-dipping method (64). At least eight independent transgenic

lines with a single T-DNA insertion were generated for each construct, and at least three independent T3 homozygous lines were used for subsequent characterization. All primers used for the generation of the constructs are listed in *SI Appendix, Table S1*.

Gene Expression and Western Blot Analyses. Total RNAs were isolated using the E.Z.N.A. Plant RNA Kit (OMEGA BioTek), and the reverse-transcription reaction was performed with a reverse transcription kit (Takara) according to the manufacturers' instructions. RT-PCR was carried out using a standard method, and transcripts of the *GLYCERALDEHYDE-3-PHOSPHATE DEHYDROGENASE C SUBUNIT 1* (*GAPC*) were used as an internal control. qRT-PCR was conducted as previously described (65), and the relative expression level of each gene was calculated using the $\Delta\Delta$ CT (cycle threshold) method. The transcript abundance of *ACTIN2* was used as an internal control. All primers used for RT-PCR and qRT-PCR are listed in *SI Appendix, Table S1*. To monitor protein abundance, the total proteins were extracted from infiltrated *N. benthamiana* leaves or homozygous transgenic *Arabidopsis* plants with a Plant Total Protein Extraction Kit (Cwbio), according to the manufacturer's instructions, and quantified by colloidal Coomassie brilliant blue. The proteins were separated by polyacrylamide gel electrophoresis and transferred onto nitrocellulose membranes, which were probed with anti-GFP (MBL) (1:5,000), anti-MYC (MBL) (1:5,000), or anti-LUC (Sigma) (1:3,000) primary antibodies, followed by HRP-labeled secondary antibody (Bioeasy; 1:10,000). Detection was performed using the ELC Super Sensitive Kit (DiNing), and the signals were captured with a Tanon 5200 imaging system. Rubisco stained with Ponceau S was used as a loading control.

Confocal Microscopy. To examine the tissue-specific or cellular accumulation of proteins, the primary roots of *Arabidopsis* seedlings harboring different GFP-tagged constructs or markers were visualized and photographed under an Olympus FV1000-MPE laser scanning microscope after being mounted in 10 mg L⁻¹ propidium iodide (Sigma). A GFP excitation/emission filter (488 nm/525 nm) was used to visualize the protein-specific fluorescence. The propidium iodide signal was visualized by excitation with an argon laser at 488 nm and detected with a spectral detector set at >585 nm for emission. The GFP fluorescent signals were quantified with ImageJ software.

Yeast Two-Hybrid Assay. The yeast two-hybrid assay was performed using the Matchmaker GAL4 two-hybrid system (Clontech). The coding sequences of *IQM5* and *CaM6* were cloned into the pGADT7 prey vector, and those of *TIR1*, *AFB2*, *AFB3*, *IAAs*, and *CaMs* were cloned into the pGBKT7 bait vector. Pairs of constructs were cotransformed into the yeast strain AH109 and grown on SD-Trp/Leu or SD-Trp/Leu/His/Ade medium supplemented with X-Gal. The primers for yeast two-hybrid constructs are listed in *SI Appendix, Table S1*.

LCI Assay. The coding sequences of *IQM1*, *IQM5*, *IAA5*, *IAA14*, *IAA19*, *IAA28*, *IAA29*, *AFB2*, and *AFB3* were fused in-frame with the N-terminal half of the

luciferase gene (NLuc) in the pCAMBIA-NLuc vector, and those of *ARF7* and *CaMs* were fused downstream of the C-terminal half of the *luciferase* gene (CLuc) in the pCAMBIA-CLuc vector (66). The NLuc- and CLuc-tagged plasmids were transformed into EHA105 followed by cotransfection into 4-wk-old *N. benthamiana* leaves via *Agrobacterium* p19 strain-mediated infiltration. After 2 d, the leaves were immersed in a fluorescein solution of 1 mM luciferin and kept in the dark for 5 min, and images were captured by the Tanon 5200 imaging system with a 10-min exposure. The proteins from the corresponding leaves were immunoblotted with the anti-LUC antibody (Sigma) (1:3,000) to determine the abundance of expressed fusion proteins. The fluorescent signals from the LCI assay were quantified by ImageJ software, and the experiments were repeated three times. The primers used for the constructs in the LCI assay are listed in *SI Appendix, Table S1*.

Co-IP Assay. For co-IP assays in *N. benthamiana* leaves and transgenic *Arabidopsis* plants, the coding sequences of *IQM5*, *CaM5*, *CaM6*, and *ARF7* fused with a *GFP* or *MYC* sequence were cloned into the pSuper1300 vector (67), and *IAA19* was cloned into the pVIPMYC binary vector (68). About 2 g of the *N. benthamiana* leaves transiently expressing proteins or 1 g of transgenic *Arabidopsis* seedlings were collected for extraction of protein. The total proteins were incubated with agarose-conjugated anti-MYC (MBL) or agarose-conjugated anti-GFP (MBL) matrix for 3 h with rotation at 4 °C. The agarose beads were washed five times with 1-mL IP buffer, and then denatured in 50 μ L of SDS loading buffer. Immunoprecipitated proteins were detected with anti-GFP antibody (MBL) (1:5,000), anti-MYC antibody (MBL) (1:5,000), and anti-LUC antibody (Sigma) (1:3,000). The experiments were repeated at least two times. All the primers used for the generation of constructs are listed in *SI Appendix, Table S1*.

Phylogenetic Analysis. Amino acid sequences of the IQM family members were obtained from TAIR (<https://www.arabidopsis.org/>), and the phylogenetic analysis was performed using the Mega X software (maximum-likelihood method, bootstrapping with 1,000 iterations, Jones-Taylor-Thornton model, uniform rates among sites, complete deletion of gaps/missing data, nearest-neighbor-interchange method).

Data Availability. All study data are included in the main text and *SI Appendix*.

ACKNOWLEDGMENTS. We thank Dr. Gerd Jürgens for providing the *DR5::GFP* seeds; Dr. Jim Haseloff for the J0121 marker line; and Dr. Legong Li for the *GCaMP6s::GFP* seeds in this study. This work was supported by the National Natural Science Foundation of China (Grants 31830055 and 32170317) and the Strategic Priority Research Program of Chinese Academy of Sciences (Grant XDB27030102).

1. K. D. Birnbaum, A. Sánchez Alvarado, Slicing across kingdoms: Regeneration in plants and animals. *Cell* **132**, 697–710 (2008).
2. K. Sugimoto, S. P. Gordon, E. M. Meyerowitz, Regeneration in plants and animals: Dedifferentiation, transdifferentiation, or just differentiation? *Trends Cell Biol.* **21**, 212–218 (2011).
3. F. Skoog, C. O. Miller, Chemical regulation of growth and organ formation in plant tissues cultured in vitro. *Symp. Soc. Exp. Biol.* **11**, 118–130 (1957).
4. D. Valvekens, M. Van Montagu, M. Van Lijsebettens, *Agrobacterium tumefaciens*-mediated transformation of *Arabidopsis thaliana* root explants by using kanamycin selection. *Proc. Natl. Acad. Sci. U.S.A.* **85**, 5536–5540 (1988).
5. R. Atta *et al.*, Pluripotency of *Arabidopsis* xylem pericycle underlies shoot regeneration from root and hypocotyl explants grown in vitro. *Plant J.* **57**, 626–644 (2009).
6. K. Sugimoto, Y. Jiao, E. M. Meyerowitz, *Arabidopsis* regeneration from multiple tissues occurs via a root development pathway. *Dev. Cell* **18**, 463–471 (2010).
7. P. Che, S. Lall, S. H. Howell, Developmental steps in acquiring competence for shoot development in *Arabidopsis* tissue culture. *Planta* **226**, 1183–1194 (2007).
8. T. Uehara, Y. Okushima, T. Mimura, M. Tasaka, H. Fukaki, Domain II mutations in *CRANE/IAA18* suppress lateral root formation and affect shoot development in *Arabidopsis thaliana*. *Plant Cell Physiol.* **49**, 1025–1038 (2008).
9. Q. Tian, J. W. Reed, Control of auxin-regulated root development by the *Arabidopsis thaliana* *SHY2/IAA3* gene. *Development* **126**, 711–721 (1999).
10. K. Tatsumatsu *et al.*, *MASSUGU2* encodes Aux/IAA19, an auxin-regulated protein that functions together with the transcriptional activator NPH4/ARF7 to regulate differential growth responses of hypocotyl and formation of lateral roots in *Arabidopsis thaliana*. *Plant Cell* **16**, 379–393 (2004).
11. T. Goh, H. Kasahara, T. Mimura, Y. Kamiya, H. Fukaki, Multiple AUX/IAA-ARF modules regulate lateral root formation: The role of *Arabidopsis* SHY2/IAA3-mediated auxin signalling. *Philos. Trans. R. Soc. Lond. B Biol. Sci.* **367**, 1461–1468 (2012).
12. H. Fukaki, Y. Nakao, Y. Okushima, A. Theologis, M. Tasaka, Tissue-specific expression of stabilized SOLITARY-ROOT/IAA14 alters lateral root development in *Arabidopsis*. *Plant J.* **44**, 382–395 (2005).
13. M. Fan, C. Xu, K. Xu, Y. Hu, LATERAL ORGAN BOUNDARIES DOMAIN transcription factors direct callus formation in *Arabidopsis* regeneration. *Cell Res.* **22**, 1169–1180 (2012).
14. H. Fukaki, S. Tameda, H. Masuda, M. Tasaka, Lateral root formation is blocked by a gain-of-function mutation in the SOLITARY-ROOT/IAA14 gene of *Arabidopsis*. *Plant J.* **29**, 153–168 (2002).
15. B. Shang *et al.*, Very-long-chain fatty acids restrict regeneration capacity by confining pericycle competence for callus formation in *Arabidopsis*. *Proc. Natl. Acad. Sci. U.S.A.* **113**, 5101–5106 (2016).
16. C. Xu *et al.*, Control of auxin-induced callus formation by bZIP59-LBD complex in *Arabidopsis* regeneration. *Nat. Plants* **4**, 108–115 (2018).
17. Y. Okushima, H. Fukaki, M. Onoda, A. Theologis, M. Tasaka, ARF7 and ARF19 regulate lateral root formation via direct activation of LBD/ASL genes in *Arabidopsis*. *Plant Cell* **19**, 118–130 (2007).
18. H. W. Lee, N. Y. Kim, D. J. Lee, J. Kim, LBD18/ASL20 regulates lateral root formation in combination with LBD16/ASL18 downstream of ARF7 and ARF19 in *Arabidopsis*. *Plant Physiol.* **151**, 1377–1389 (2009).
19. W. Tian, C. Wang, Q. Gao, L. Li, S. Luan, Calcium spikes, waves and oscillations in plant development and biotic interactions. *Nat. Plants* **6**, 750–759 (2020).
20. V. S. Reddy, G. S. Ali, A. S. N. Reddy, Genes encoding calmodulin-binding proteins in the *Arabidopsis* genome. *J. Biol. Chem.* **277**, 9840–9852 (2002).
21. N. Bouché, A. Yellin, W. A. Snedden, H. Fromm, Plant-specific calmodulin-binding proteins. *Annu. Rev. Plant Biol.* **56**, 435–466 (2005).
22. S. Zhang *et al.*, *Arabidopsis* CNGC14 mediates calcium influx required for tip growth in root hairs. *Mol. Plant* **10**, 1004–1006 (2017).
23. W. Tian *et al.*, A calmodulin-gated calcium channel links pathogen patterns to plant immunity. *Nature* **572**, 131–135 (2019).

24. Y. Pan *et al.*, Dynamic interactions of plant CNGC subunits and calmodulins drive oscillatory Ca²⁺ channel activities. *Dev. Cell* **48**, 710–725.e5 (2019).
25. W. Zhang *et al.*, Molecular and genetic evidence for the key role of AtCaM3 in heat-shock signal transduction in Arabidopsis. *Plant Physiol.* **149**, 1773–1784 (2009).
26. Y. Xuan, S. Zhou, L. Wang, Y. Cheng, L. Zhao, Nitric oxide functions as a signal and acts upstream of AtCaM3 in thermotolerance in Arabidopsis seedlings. *Plant Physiol.* **153**, 1895–1906 (2010).
27. J. Yang *et al.*, The CaM1-associated CcAMK-MKK1/6 cascade positively affects lateral root growth via auxin signaling under salt stress in rice. *J. Exp. Bot.* **72**, 6611–6627 (2021).
28. Y. P. Zhou *et al.*, Arabidopsis IQM4, a novel calmodulin-binding protein, is involved with seed dormancy and germination in Arabidopsis. *Front Plant Sci* **9**, 721 (2018).
29. Y. P. Zhou, J. Duan, T. Fujibe, K. T. Yamamoto, C. E. Tian, AtIQM1, a novel calmodulin-binding protein, is involved in stomatal movement in Arabidopsis. *Plant Mol. Biol.* **79**, 333–346 (2012).
30. T. Lv *et al.*, The calmodulin-binding protein IQM1 interacts with CATALASE2 to affect pathogen defense. *Plant Physiol.* **181**, 1314–1327 (2019).
31. L. P. Gong, J. Z. Cheng, Y. P. Zhou, X. L. Huang, C. E. Tian, Disruption of IQM5 delays flowering possibly through modulating the juvenile-to-adult transition. *Acta Physiol. Plant.* **39**, 21 (2017).
32. T. Thorpe, History of plant tissue culture. *Methods Mol. Biol.* **877**, 9–27 (2012).
33. L. Laplaze *et al.*, GAL4-GFP enhancer trap lines for genetic manipulation of lateral root development in Arabidopsis thaliana. *J. Exp. Bot.* **56**, 2433–2442 (2005).
34. V. Arondel *et al.*, Map-based cloning of a gene controlling omega-3 fatty acid desaturation in Arabidopsis. *Science* **258**, 1353–1355 (1992).
35. Y. Zhou, Y. Chen, K. T. Yamamoto, J. Duan, C. E. Tian, Sequence and expression analysis of the Arabidopsis IQM family. *Acta Physiol. Plant.* **32**, 1235–1235 (2010).
36. Y. Zhou *et al.*, Initial characterization of Arabidopsis T-DNA insertion mutants of the IQM1 gene that encodes an IQ Motif containing protein. *Plant Cell Physiol.* **48**, S197–S197 (2007).
37. N. A. Al-Quraan, R. D. Locy, N. K. Singh, Expression of calmodulin genes in wild type and calmodulin mutants of Arabidopsis thaliana under heat stress. *Plant Physiol. Biochem.* **48**, 697–702 (2010).
38. J. Chen, L. Xia, M. R. Bruchas, L. Solnica-Krezel, Imaging early embryonic calcium activity with GCaMP6s transgenic zebrafish. *Dev. Biol.* **430**, 385–396 (2017).
39. J. Friml *et al.*, Efflux-dependent auxin gradients establish the apical-basal axis of Arabidopsis. *Nature* **426**, 147–153 (2003).
40. E. J. Chapman, M. Estelle, Mechanism of auxin-regulated gene expression in plants. *Annu. Rev. Genet.* **43**, 265–285 (2009).
41. A. Delbarre, P. Muller, V. Imhoff, J. Guern, Comparison of mechanisms controlling uptake and accumulation of 2,4-dichlorophenoxy acetic acid, naphthalene-1-acetic acid, and indole-3-acetic acid in suspension-cultured tobacco cells. *Planta* **198**, 532–541 (1996).
42. M. Salehin, R. Bagchi, M. Estelle, SCFTIR1/AFB-based auxin perception: Mechanism and role in plant growth and development. *Plant Cell* **27**, 9–19 (2015).
43. O. Leyser, Auxin signaling. *Plant Physiol.* **176**, 465–479 (2018).
44. H. Li, S. B. Tiwari, G. Hagen, T. J. Guilfoyle, Identical amino acid substitutions in the repression domain of auxin/indole-3-acetic acid proteins have contrasting effects on auxin signaling. *Plant Physiol.* **155**, 1252–1263 (2011).
45. T. Ulmasov, G. Hagen, T. J. Guilfoyle, ARF1, a transcription factor that binds to auxin response elements. *Science* **276**, 1865–1868 (1997).
46. D. A. Korasick *et al.*, Molecular basis for AUXIN RESPONSE FACTOR protein interaction and the control of auxin response repression. *Proc. Natl. Acad. Sci. U.S.A.* **111**, 5427–5432 (2014).
47. A. Iwase *et al.*, The AP2/ERF transcription factor WIND1 controls cell dedifferentiation in Arabidopsis. *Curr. Biol.* **21**, 508–514 (2011).
48. M. Ikeuchi, K. Sugimoto, A. Iwase, Plant callus: Mechanisms of induction and repression. *Plant Cell* **25**, 3159–3173 (2013).
49. P. Che, S. Lall, D. Nettleton, S. H. Howell, Gene expression programs during shoot, root, and callus development in Arabidopsis tissue culture. *Plant Physiol.* **141**, 620–637 (2006).
50. A. J. Trethewas, R. Malhó, Ca²⁺ signalling in plant cells: The big network! *Curr. Opin. Plant Biol.* **1**, 428–433 (1998).
51. L. Steinhorst, J. Kudla, Signaling in cells and organisms—Calcium holds the line. *Curr. Opin. Plant Biol.* **22**, 14–21 (2014).
52. D. E. Clapham, Calcium signaling. *Cell* **131**, 1047–1058 (2007).
53. H. Zhang *et al.*, A plant phytosulfokine peptide initiates auxin-dependent immunity through cytosolic Ca²⁺ signaling in tomato. *Plant Cell* **30**, 652–667 (2018).
54. T. Li *et al.*, Calcium signals are necessary to establish auxin transporter polarity in a plant stem cell niche. *Nat. Commun.* **10**, 726 (2019).
55. V. Tripathi, N. Syed, A. Laxmi, D. Chattopadhyay, Role of CIPK6 in root growth and auxin transport. *Plant Signal. Behav.* **4**, 663–665 (2009).
56. V. Tripathi, B. Parasuraman, A. Laxmi, D. Chattopadhyay, CIPK6, a CBL-interacting protein kinase is required for development and salt tolerance in plants. *Plant J.* **58**, 778–790 (2009).
57. B. Singla, A. Chugh, J. P. Khurana, P. Khurana, An early auxin-responsive Aux/IAA gene from wheat (*Triticum aestivum*) is induced by epibrassinolide and differentially regulated by light and calcium. *J. Exp. Bot.* **57**, 4059–4070 (2006).
58. T. Yang, B. W. Poovaliah, Molecular and biochemical evidence for the involvement of calcium/calmodulin in auxin action. *J. Biol. Chem.* **275**, 3137–3143 (2000).
59. S. Vanneste, J. Friml, Calcium: The missing link in auxin action. *Plants* **2**, 650–675 (2013).
60. R. J. DiDonato *et al.*, Arabidopsis ALF4 encodes a nuclear-localized protein required for lateral root formation. *Plant J.* **37**, 340–353 (2004).
61. R. Bagchi *et al.*, The Arabidopsis ALF4 protein is a regulator of SCF E3 ligases. *EMBO J.* **37**, 255–268 (2018).
62. M. Ruegger *et al.*, Reduced naphthylphthalamic acid binding in the *tir3* mutant of Arabidopsis is associated with a reduction in polar auxin transport and diverse morphological defects. *Plant Cell* **9**, 745–757 (1997).
63. Z. P. Wang *et al.*, Egg cell-specific promoter-controlled CRISPR/Cas9 efficiently generates homozygous mutants for multiple target genes in Arabidopsis in a single generation. *Genome Biol.* **16**, 144 (2015).
64. S. J. Clough, A. F. Bent, Floral dip: A simplified method for Agrobacterium-mediated transformation of Arabidopsis thaliana. *Plant J.* **16**, 735–743 (1998).
65. K. J. Livak, T. D. Schmittgen, Analysis of relative gene expression data using real-time quantitative PCR and the 2⁻(Delta Delta C(T)) method. *Methods* **25**, 402–408 (2001).
66. C. Liu *et al.*, Two Arabidopsis receptor-like cytoplasmic kinases SZE1 and SZE2 associate with the ZAR1-ZED1 complex and are required for effector-triggered immunity. *Mol. Plant* **12**, 967–983 (2019).
67. V. Chinnusamy *et al.*, ICE1: A regulator of cold-induced transcriptome and freezing tolerance in Arabidopsis. *Genes Dev.* **17**, 1043–1054 (2003).
68. Y. Hu, Q. Xie, N. H. Chua, The Arabidopsis auxin-inducible gene ARGOS controls lateral organ size. *Plant Cell* **15**, 1951–1961 (2003).